# Transcriptomic Profiling of JEG-3 cells using human leiomyoma derived matrix

Barmaki, Samineh

2022-08-07

# Transcriptomic Profiling of JEG-3 cells using human leiomyoma derived matrix

Samineh Barmaki [a,*], Ahmed Al-Samadi [b,1], Katarzyna Leskinen [c,1], Wafa Wahbi [a], Ville Jokinen [d], Sanna Vuoristo [e], Tuula Salo [b], Juha Kere [f,g,h], Satu Wedenoja [e,i,2], Päivi Saavalainen [c,g,2]

a Department of Pharmacology, Faculty of Medicine, University of Helsinki, Helsinki 00290, Finland
b Department of Oral and Maxillofacial Disease, University of Helsinki, Helsinki 00290, Finland
c Translational Immunology Research Program, and Department of Clinical and Medical Genetics, University of Helsinki, Helsinki 00290, Finland
d Department of Chemistry and Materials Science, School of Chemical Engineering, Aalto University, Espoo 00076, Finland
e Obstetrics and Gynecology, University of Helsinki and Helsinki University Hospital, Helsinki 00290, Finland
f Department of Biosciences and Nutrition, Karolinska Institutet, Huddinge 14183, Sweden
g Folkhälsan Research Center, Helsinki 00290, Finland
h Stem Cells and Metabolism Research Program, University of Helsinki, Helsinki 00014, Finland
i Stem Cells and Metabolism Research Program, University of Helsinki, and Folkhälsan Research Center, Helsinki 00290, Finland

## ARTICLE INFO

## ABSTRACT

Oxygen tension varies during placental and fetal development. Although hypoxia drives early trophoblast invasion, low placental oxygen levels during pregnancy show association with pregnancy complications including fetal growth restriction and preeclampsia. JEG-3 cells are often used as a trophoblast model. We studied transcriptional changes of JEG-3 cells on a uterine leiomyoma derived matrix Myogel. This might be the closest condition to the real uterine environment that we can get for an in vitro model. We observed that culturing JEG-3 cells on the leiomyoma matrix leads to strong stimulation of ribosomal pathways, energy metabolism, and ATP production. Furthermore, Myogel improved JEG-3 cell adherence in comparison to tissue culture treated plastic. We also included PDMS microchip hypoxia creation, and observed changes in oxidative phosphorylation, oxygen related genes and several hypoxia genes. Our study highlights the effects of Myogel matrix on growing JEG-3 cells, especially on mitochondria, energy metabolism, and protein synthesis.

## 1. Introduction

Trophoblasts are temporary cells that form the epithelial layer of the placenta. Deep invasion of fetal trophoblasts into the uterine wall of the mother is a crucial step of the placentation to deliver adequate blood and oxygen supply to the fetus. Defects in the trophoblast invasion during early pregnancy limit the placental development and capacity and might underlie a spectrum of human pregnancy complications, from miscarriages to fetal growth restriction and preeclampsia [1].

Many problems in human pregnancy show association with chronic placental hypoxia. Early stages of placentation are also accompanied with a decline in the oxygen levels at the maternal-fetal interface. This physiological hypoxia results in deeper invasion of extravillous trophoblasts into the wall of the uterus in search for oxygen, and formation and remodeling of the spiral arteries. In later stages of human pregnancy, however, trophoblasts are unable to invade and pla-

cental hypoxia leads to inflammation, oxidative stress, and apoptosis [2–9].

Studying the earliest stages of placentation remains challenging. There are several reason for it. First, primary trophoblasts isolated from human first-trimester placentas do not proliferate in vitro [10]. Second, different hypoxia systems such as low-oxygen chambers and chemicals provide partly inconsistent findings [11]; and finally, the medium used in hypoxia experiments may further modify cellular responses [12]. To date, many studies have utilized JEG-3 chorioncarcinoma cell line as a model for early trophoblasts [10,13–15].

Hypoxia-induced changes in JEG-3 cells involve reduction of the major placental hormone human chorionic gonadotropin (hCG), upregulation of the vascular endothelial growth factor (VEGF) [8,10], and transcriptional regulation of a number of other genes by Hypoxia Inducible Factors (HIFs) [16]. However, results vary depending on the applied hypoxia system [17–21].

---

* Corresponding author.
  E-mail addresses: samineh.barmaki@helsinki.fi (S. Barmaki), paivi.saavalainen@helsinki.fi (P. Saavalainen).
1 These authors contributed equally to this work.
2 These authors contributed equally to this work.

We have previously generated a microfluidic chip setup, where hypoxia is generated by pumping oxygen scavenger solution into a microfluidic channel that is separated from the cell culture by a gas-permeable membrane [22,23].

We hypothesized that this system could be used to model hypoxia-induced gene expression changes of human trophoblast.

We studied RNA expression of JEG-3 cells using the hypoxia microchip we developed, and human leiomyoma- derived matrix Myogel, which mimics tumor micro-environment and the human uterine wall [24,25]. Also, we present cellular responses and the genes that are differentially expressed during hypoxia, and the utility of Myogel as an extracellular matrix for the JEG-3 culture.

## 2. Materials and methods

### 2.1. Cell culture

All experiments were performed using JEG-3 cells (RRID: CVCL-0363). These cells were cultured using Eagles minimum essential medium[3] with non-essential amino acids, 90% sodium pyruvate, and 10% antibiotic-free Fetal bovine serum (FBS, Gibco). Cells from passages 5–12 were used for experiments. All cell culture experiments were performed using a regular cell incubator (37° with 5% $CO_2$).

### 2.2. Testing different coating on JEG-3 cells

24-well plates[4] were coated with poly-dimethyl-siloxane (PDMS). PDMS consists of two parts of polymer (Base Elastomer and Curing Agent). We used the standard mixing ration for PDMS, 10 parts base elastomer and 1 part curing agent $(10 : 1)$ to coat the cell culture well plates. Then $150\mu l$ of PDMS added to the 24 well plates (surface area: $1.9 cm^2$). We used the same PDMS ratio $(10 : 1)$ to fabricate our previous reported microchips and the PDMS membrane).

Then, 0.5 mg/ml Myogel (50ôl/well) and/or fibrin matrix were added on PDMS, while control wells remained uncoated. For stabilizing the coating, the plates were incubated in 37° with 5% $CO_2$ for 24 hours. JEG-3 cells were seeded 24 hours after coating of the plates. The cells were lysed after the first and third day for RNA analysis. All experiments were performed in three technical replicates.

We collected the cells on day 1 and day 3 to evaluate RNA concentrations. Because of the observed increase in RNA yields from day 1 to 3, and for the normal morphology of cells on day 1, we then performed RNA analyses on day 1 cells. Moreover, for the hypoxia experiment, we used an incubation time of 24 hours (day 1), which has been used in several earlier hypoxia studies on JEG-3 cells [9,26].

### 2.3. PDMS microchip fabrication

The PDMS chips were fabricated by replication molding from SU-8 masters. The fabrication method and design of the microfluidic chips have been described previously [22]. Briefly: The SU-8[5] was spin coated 4000 rpm 30s for a $40\mu m$ thick layer. The chips were made from PDMS[6] with the ratio of 10:1 with the cross-linking agent. The chips were closed by bonding a $30\mu m$ thick PDMS membrane on top of the channels. The PDMS membrane was fabricated by spin coating PDMS $2000 rpm$ $30s$ on top of an anti-adhesive fluoropolymer coats silicon wafer.

### 2.4. Microchip assay

The surface adherence plays essential role in PDMS attachment on PDMS reservoir [27]. The microfluidic chips and cell reservoir were

washed gently with soap and rinsed with deionized water and 70% ethanol. Then, they were dried with pressurized air; a piece of scotch tape was used to remove any residual dust or particles from the surface. For testing the functionality of microfluidics before cell culture experiments, water was pumped with a microfluidic syringe pump[7] with flow rate of $0.1 ml/h$ $(1.6\mu l/min)$ into the microfluidic channels. If any leaks was detected during the test the chip is discarded.

A 2D cell culture matrix with Myogel was generated on PDMS membrane of microfluidic chip. The oxygen scavenger solution was pumped for $24 hours$ in the two meanders of the microchip with the flow rate of $0.1 ml/h$. Hypoxia was induced on the cells that were separated from an underlying oxygen scavenging channel network by a thin PDMS membrane, as described previously [22,23].

For making oxygen scavenger solution a water solution of sodium sulfite ($835 mM$ oxygen-depleted $H_2O$) was used to generate the oxygen sink. The reaction of sodium sulphite ($Na_2SO_3$) with dissolved oxygen in $H_2O$ is utilized for oxygen depletion and generation of an active in-liquid oxygen sink. Cobalt nitrate ($Co(NO_3)_2$ hexahydrate salt, $9 mM$) in nitric acid was used as the catalyst. All reagents were obtained from Sigma Aldrich[8]. Fig. 1 illustrates the structure of the hypoxia microchip, where hypoxia was generated by pumping of the oxygen scavenger solution in the microfluidic channels under the JEG-3 cells.

### 2.5. RNA-sequencing and data analysis

RNA was extracted from the JEG-3 cells using the RNA easy Mini Kit[9] according to the manufacturers instructions. Cells were homogenized with QIAshredder columns (Qiagen). After extraction, RNA was quantified using Qubit 2 Fluorometer[10] with the Qubit RNA HS Assay Kit[11]. RNA samples were stored at $-70°C$. The RNA sequencing method was designed based on the Drop-seq. protocol, as described [20]. Briefly speaking, $10 ng$ of RNA was mixed with Indexing Oligonucleotides[12]. After 5 minutes of incubation at ambient temperature, RNA was combined with RT mix containing $1\times$ Maxima RT buffer, $1 mM$ dNTPs, $10 U/\mu l$ Maxima HRTase, $1 U/\mu l$ RiboLock[13], and $2.5\mu M$ Template Switch Oligo[14]. Samples were incubated in a T100 thermal cycler[15] for 30 minutes at $22°C$ and 90 minutes at $52°C$. The constructed cDNA was amplified by PCR in a volume of $15\mu l$ using $5\mu l$ of RT mix as template, $1\times$ HiFi HotStart Ready-mix[16], and $0.8\mu M$ SMART PCR primer. The samples were thermo-cycled in a T100 thermocycler as follows: $95°C$ 3 min; subsequently four cycles of $98°C$ for 20 sec, $65°C$ for 45 sec, $72°C$ for 3 min; following 16 cycles of $98°C$ for 20 sec, $67°C$ for 20 sec, $72°C$ for 3 min; and with the final extension step of 5 min at $72°C$. The PCR products were pooled together in sets of 27 samples containing different Indexing Oligos and purified with 0.6X High-Prep PCR Clean-up System[17] according to the manufacturers instructions. They were eluted in $10\mu l$ of molecular grade water. The 3-end cDNA fragments for sequencing were prepared using the Nextera XT[18] tagmentation reaction with $1 ng$ of each PCR product serving as an input. The reaction was performed according to the manufacturers instructions, with the exception that the P5 SMART primer was used instead of the i5 Nextera primer. After the PCR reaction, each set of samples was pooled and

---

[3] MEM, Gibco, Thermo Fisher Scientific Inc, Waltham, MA
[4] Thermo Fisher Scientific Inc, Waltham, MA
[5] SU-8 50, Kayaku Advanced Materials, Westborough, MA
[6] Sylgard 184, Merck, KGaA, Darmstadt, Germany

[7] NE-4000, New Era Pump Systems Inc., Farmingdale, NY
[8] St. Louis, MA
[9] Qiagen, Hilden, Germany
[10] ThermoFisher Scientific
[11] ThermoFisher Scientific
[12] Integrated DNA Technologies
[13] ThermoFisher Scientific
[14] TSO, Integrated DNA Technologies
[15] BioRad, Hercules, California, United States
[16] Kapa Biosystems, Massachusetts, United States
[17] MagBio, Gaithersburg, Maryland, United States
[18] Illumina, San Diego, United States

**Fig. 1.** Structure of the hypoxia microchip.



1. Media
2. JEG-3 Cells
3. Myogel
4. PDMS membrane (30μm)
5. Microfluidic channel
6. Oxygen scavanger solution

Pumping oxygen scavanger solution to generate hypoxia microenvironmnet in cells

tagmented with a different Nextera i7 index. Subsequently, the samples were PCR amplified as follows: 95°C for 30 sec; 11 cycles of 95°C for 10 sec, 55°C for 30 sec, 72°C for 30 sec; with the final extension step of 5 min at 72°C. Samples were purified twice using $0.6\times$ and $1.0\times$ High-Prep PCR Clean-up System (MagBio) and eluted in $10\mu l$ of molecular grade water.

The concentration of the library was measured using a Qubit 2 Fluorometer[19] and the Qubit DNA HS Assay Kit[20], while the quality was assessed using the LabChip GXII Touch HT electrophoresis system[21], with the DNA High Sensitivity Assay (PerkinElmer) and the DNA 5K/RNA/Charge Variant Assay LabChip (PerkinElmer). Samples were stored at $-20°C$. The libraries were sequenced on an Illumina NextSeq 500, with an addition of the custom primer producing a read 1 of $20bp$ and a read 2 (paired end) of $55bp$. Sequencing was performed at the Functional Genomics Unit of the University of Helsinki. The RNA sequencing data has been deposited to NCBI Gene Expression Omnibus (Accession ID: GSE182988).

Raw sequence data was filtered to remove reads shorter than $20bp$. Subsequently, the original pipeline for processing of Drop-seq data was used [28]. Briefly, reads were additionally filtered to remove poly A tails of length 6 or greater, and aligned to the human (GRCh38) genome using STAR aligner with default settings [29]. Uniquely mapped reads were grouped according to the barcodes 1 to 9, and gene transcripts were counted by their Unique Molecular Identifiers (UMIs) to reduce bias emerging from the PCR amplification. Digital expression matrices (DGE) were used for reporting the number of transcripts per gene in each sample (according to the distinct UMI sequences counted). Differentially expressed genes were identified using DESeq2 [30] with the cut-off for the adjusted p-value set to 0.05. We compared our hypoxia microchip data on JEG-3 RNA expression with an independent publicly available dataset. RNA-seq data on expression of JEG-3 cells cultured in a hypoxia chamber for 24 hours [31] were downloaded from the GEO under the accession number GSM1862652.

Normalization and differential expression analysis between these two data sets were performed using edgeR [32] package integrated into Chipster platform [33]. Heatmaps were drawn with heatmapper tool [34] and pathway analyses were performed with Enrichr (MSigDB Hallmark 2020 pathway) [35,36].

## 3. Results

### 3.1. Influence of Myogel coating on gene expression and cell morphology

We assessed the morphology and RNA expression of JEG-3 cells at the first day of the cell culture. We compared cell morphology and an-

alyzed gene expression of the JEG-3 cells cultured in the wells coated with Myogel, PDMS, Myogel + PDMS, Myogel + fibrin, Myogel + fibrin + PDMS, and uncoated control, (Fig. 3). Total RNA yields increased in extractions from day one to day 3 (Supplementary Table S10), indicating that the cells were proliferating. The genes and corresponding pathways modulated by different conditions were studied. Some of the most significant findings were in association with Myogel coating, (Table 1 ; Fig. 2). When Myogel was added to the JEG-3 culture, 308 genes showed differential expression (Supplementary Table S2), and Myogel provided better cell adhesion (Fig. 3c).

The gene expression changes that were observed were related to several neurological diseases (Huntington disease, Parkinson disease, and Alzheimer disease). This might reflect the crucial role of oxygen supply in different tissues, including both the placenta and brain. This finding indicates that the changes we observed were not trophoblast specific but more related to general changes in energy metabolism. These pathways were tightly related to several NDUF genes (NDUFB7; NDUFB3; NDUFB; NDUFV1) mitochondrial respiratory genes, and ribosomal protein metabolism. We also assessed how PDMS and fibrin - or their combinations - modulate gene expression when they were used with Myogel. When the cells were coated with the combination of Myogel, fibrin, and PDMS, we observed significant modulation of ribosomal genes. This observation was similar to what has been seen with pure Myogel; accordingly, fibrin itself has very small effects on gene expression, (Table 1, Fig. 2). This was particularly demonstrated between the conditions PDMS + Myogel vs. PDMS + fibrin + Myogel, showing almost no changes in gene expression. However, the comparison between Myogel + fibrin + PDMS vs. PDMS only produced significant changes in gene expression (Table 1, Figs. 2 and 3).

Although the Myogel culture-associated pathways indicated significant changes, single genes were not changed to the same extent. Analysis of differentially expressed genes revealed upregulation of hypoxia pathway with two genes associated with PDMS coating vs. control: EFNA1 and SLC2A1 (P-value: 0.016), (see Fig. 2). This may be caused by hydrophobic surface property of PDMS that induces organoid type of structures (Fig. 3b), suggesting that oxygen might not diffuse freely in the cells. However, hypoxic pathway was also up-regulated by Myogel vs. pure medium, as seen about the genes EFNA1, SLC25A1, BTG1, ANXA2, and CAV1 (P-value: 0.196). Interestingly, adding Myogel on the PDMS coated culture prevented the development of organoid structures (see Fig. 3d), but showed no clear changes in gene expression. In contrast, adding fibrin to Myogel-coated culture resulted in no changes in gene expression, but three dimensional organization of the cells was observed (Fig. 3e).

Detailed information of well-plate experiment, such as DE-gene lists (Supplementary Tables S3-S9) and significant genes in one heat-map (see Supplementary Figure S3) with Venn diagram of important pathways of well-plate experiment (Supplementary Figure S4) showed in the supplementary section.

---

[19] ThermoFisher Scientific
[20] ThermoFisher Scientific
[21] PerkinElmer, Waltham, Massachusetts, United States

**Table 1**

Up-regulated Pathways of JEG cells on well plate experiment.

| PDMS *v.s.* Control | | | Myogel *v.s.* Control | | |
|---|---|---|---|---|---|
| Term | P-value | Genes | Term | P-value | Genes |
| Coagulation | 0.008 | CRIP2; CTSV | Oxidative Phosphorylation | ≈ 0 | COX7B; SLC25A3; ECHS1; NDUFB7; NDUFB3; NDUFB; NDUFV1; ATP5G; ATP5ME; COX8A; TIMM8B; ATP5P |
| Mitotic Spindle | 0.016 | CEP131; SPTBN1 | Myc Targets V1 | ≈ 03 | DDX18; SLC25A3; CNBP; RPLP0; ILF2; SRPK1; LSM2; PSMD8; CDC20; AIMP2; SYNCRIP; FBL; LSM7; C1QBP; NDUFAB1; POLD2; RACK1; SRSF2; SNRPG; SRSF7; EIF4G2 |
| Hypoxia | 0.016 | EFNA1; SLC2A1 | Adipogenesis | ≈ 0 | COX8A; SLC25A1; COX7B; MTCH2; ECHS1; NDUFB7; ITSN1; ECH1; TALDO1; CHCHD10; UQCR11; ATP1B3; MRPL15; UQCR10; UQCRQ; NDUFAB1; UQCRC1; SUCLG1 |
| Estrogen Response Late | 0.016 | ATP2B4; EMP2 | E2F Targets | 0.001 | CDC20; SYNCRIP; ILF3; POP7; POLD2; SRSF2; PSIP1; MKI67; DCTPP1; RAN |
| TGF-beta Signaling | 0.052 | SPTBN1 | Peroxisome | 0.001 | FDPS; VPS4B; CNBP; ECH1; SLC25A4; FADS1; YWHAH |
| PI3K / AKT / mTOR Signaling | 0.099 | SLC2A1 | Myc Targets V2 | 0.001 | DDX18; AIMP2; PPAN; FARSA; DCTPP1 |
| UV Response Dn | 0.134 | ATP2B4 | Fatty Acid Metabolism | 0.003 | ECHS1; NTHL1; UROS; ECH1; SUCLG1; PRDX6; HSD17B10; YWHAH |
| UV Response Up | 0.146 | CTSV | G2-M Checkpoint | 0.003 | CDC20; TPX2; SYNCRIP; PRMT5; GINS2; ILF3; UBE2C; SRSF2; MKI67 |
| IL-2 / STAT5 Signaling | 0.181 | CD81 | Cholesterol Homeostasis | 0.005 | FDPS;EBP;ECH1; HMGCR; S100A11 |
| TNF-alpha Signaling via NF-kB | 0.182 | EFNA1 | Unfolded Protein Response | 0.008 | RPS14; NOP14; EXOSC4; IMP3; POP4; HSP90B1 |
| p53 Pathway | 0.182 | CD81 | DNA Repair | 0.028 | NT5C; MPG; ELOA; SAC3D1; ITPA; POLR2K |
| heme Metabolism | 0.182 | SLC2A1 | Androgen Response | 0.068 | KRT19; UBE2I; HMGCR; FADS1 |
| Estrogen Response Early | 0.182 | SLC2A1 | Estrogen Response Late | 0.09 | CDC20; GINS2; KRT19; PERP; CAV1; DCXR |
| Complement | 0.182 | CTSV | mTORC1 Signaling | 0.09 | CCT6A; EBP; HMGCR; FADS1; HSP90B1; ATP5MC1 |
| mTORC1 Signaling | 0.1821 | SLC2A1 | p53 Pathway | 0.09 | LDHB; BTG1; PERP; DCXR; RGS16; RACK1 |
| Epithelial Mesenchymal Transition | 0.182 | MFAP5 | UV Response Up | 0.09 | NFKBIA; EIF5; BTG1; EPCAM; SLC25A4 |
| | | | Reactive Oxygen Species Pathway | 0.17 | NDUFA6; PRDX6 |
| | | | Protein Secretion | 0.18 | SGMS1; VPS4B;CLTA |
| | | | Mitotic Spindle | 0.193 | TPX2; PPP4R2; ITSN1; CKAP5; SAC3D1 |
| | | | Hypoxia | 0.196 | EFNA1; SLC25A1; BTG1; ANXA2; CAV1 |

### 3.2. *Genes and pathways in Myogel coated hypoxia microchip*

The data suggested that Myogel enhances cell adherence on PDMS, without inducing changes in gene expression. The cell adhesion was visually suspected because they were tightly adherent, when collected for RNA extraction. These results prompted us to use Myogel coating on PDMS microchips in hypoxia experiments. We assessed the genes and pathways that were modulated in Myogel coated PDMS microchips and exposed to oxygen scavenger for 24 hours. The chip generates oxygen levels of < 5%, as shown in our previous study, through the activation of image-iT® red fluorescent marker. Because of the formation of organoid structures, we could not use pure PDMS as a control in these experiments, (see Fig. 3a and b). We used Myogel on PDMS microchip, as we observed that PDMS had no effect on gene expression when it was used in addition to Myogel, (Fig. 3c and d). Moreover, liquid form of pure Myogel, in contrast with respect to the thick gel formed with fibrin, allowed the cells to adhere on the PDMS membrane as a single layer, exposing the cells evenly to hypoxia.

In normoxia, the cells were cultured on a microchip pumped with water, whereas in hypoxia, the microchip was pumped with oxygen scavenger solution for 24 hours. Principal component analysis (PCA) of samples cultured under hypoxia or normoxia samples microchips revealed a clear separation between the samples, as expected (Supplementary Figure S1).

### 4. Discussion

Ribosome biosynthesis, the top pathway modulated by JEG-3 cells cultured on Myogel, plays a role in protein synthesis, cell growth, and tumorigenesis [35]. Our findings indicate significant metabolic changes when Myogel was used as a matrix of a JEG-3 cell culture. These data

suggest that Myogel promotes JEG-3 cells growth and differentiation, and regulates pathways that are associated with human diseases.

Adding PDMS on Myogel + fibrin coating showed no obvious changes in cell morphology and no organoid structures, but 36 genes were up-regulated. Collectively, these morphological findings are in line with the previous observations, showing that Myogel provides better cell migration, and Myogel + fibrin coating generates two and three dimensional matrices [24,25,36]. Considered together, these data indicate that the coating has a marked impact on gene expression and morphology, including key cellular processes such as ribosome biosynthesis (mainly Myogel related effect), endocytosis, and adhesion-associated genes such as several of the matrix metalloproteases [37,38]. The main pathways that were repressed by hypoxia microchip included mTOR (Mammalian target of rapamycin), MYC (Myelocytomatosis oncogene), E2F (Early 2 factor), and oxidative phosphorylation. Because MYC is a major cell proliferation marker, upregulation of MYC together with G2M checkpoint support that the cells start to proliferate faster in response to hypoxia, see Supplementary Figure S2. These findings point toward reprogramming of cancer cell metabolism, tumor cell growth and progression, and mitochondrial metabolism [38–43].

We observed altogether 306 differentially expressed genes in JEG-3 cells in hypoxia vs. normoxia (Supplementary Table S1), including upregulation of the mitochondrially encoded genes such as MT-RNR2, MT-ND4, MT-CO2, and MT-CYB, and the lncRNA gene MALAT1. These genes play key roles in mitochondria metabolism, which might reflect the effects of the limited oxygen availability [44]. The most significantly down-regulated genes during hypoxia included UQCR11, IP6K1, STK17A, NFE2L2, and C1QBP. These genes activated oxidative stress, MYC targets (v1,v2), and TNF alpha/NF-kB, all of which modulate cell proliferation, differentiation, apoptosis and coagulation [45–51].
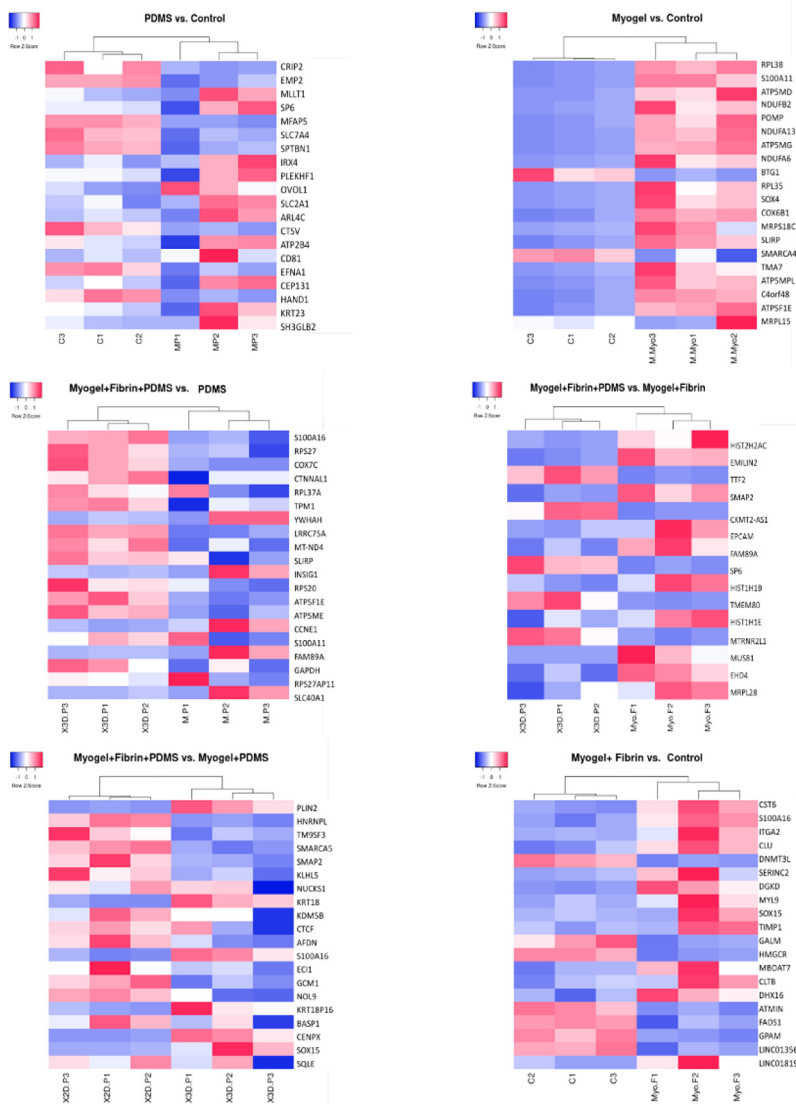
**Fig. 2.** Comparison of differentially expressed genes between the well plates coated with PDMS, Myogel, fibrin, and their combinations. Heat-maps show the top 20 differentially expressed genes (with 2-fold change or greater) in JEG-3 cells for each conditions after hierarchical clustering analysis. Each column represents three replicates for each of the two conditions (M.P: PDMS, C: Control, Myo.F: Myogel + Fibrin (Myo: Myogel, F: Fibrin), X3D.P: Myogel + Fibrin + PDMS,(X3D: Myogel+Fibrin, P: PDMS) X2D.P: Myogel + PDMS (X2D:Myogel,P: PDMS), M.Myo : Myogel), and the rows indicate the genes. The gene expression levels were shown by color and intensity: red indicates down-regulation and blue up-regulation, and higher color intensity reflects higher fold change. Statistical analysis done by heatmapper, Three replicates from each condition, (n=3). (For interpretation of the references to colour in this figure legend, the reader is referred to the web version of this article.)

Although the pathways associated with cell proliferation were activated in response to oxygen scavenger, we found no significant enrichment of the hypoxia pathway genes in the Enrichr pathway analysis. However, five individual hypoxia related genes showed significant upregulation: AKAP12, TPI1, ZNF292, ENO1, and GAPDH. We further compared our genes and pathways modulated in the hypoxia microchip experiment by reanalyzing the results of Zhu et al. [52]. They have studied the effect of hypoxia using JEG-3 cells in a hypoxia chamber for 16 hours. In their experiment, 131 genes were differentially expressed. Of these genes, 14 were differentially expressed also on our microchip, and 12 of these showed effects to the same direction, although the expression fold changes were smaller with our microchip (see Table 2). The most important pathways that were linked to differentially express genes in both our study and by Zhu et al. were oxidative phosphorylation, E2F targets, P53 pathways, apoptosis, hypoxia, and PI3K/AKT/mTOR signaling. Altogether, our study found genes from 33 shared pathways that were observed in the study of Zhu et al.,see Supplementary Table S2. Notably, MYC pathway was similarly enriched in both studies. Although only few genes from hypoxia pathway were observed in our microchip experiment, we observed changes in the expression of mitochondrial genes (MT-RNR2, MT-ND4, MT-CO2, and MT-CYB). This could be related to oxidative stress and reflect the cellular environment in our experiment.

The non-significant effects of our microchip on hypoxia pathway might be related to Myogel, microchip setup, or the duration and the level of hypoxia. In contrast with hypoxic chambers, our microchip involves oxygen deprivation from the apical surface of the cells, which is in contact with the PDMS membrane. It is therefore possible that the luminal side of the cells gets more oxygen from the culture media, and results in only a modest change of hypoxia induced gene expression. The other possibility for the insufficient hypoxia response on our microchip setup could be the chemical reactions of the oxygen scavenger solution. Hypoxic condition are generated by the conversion of sodium sulphite to sodium sulphate (Eq. 1) [53]. Furthermore, sodium sulphite generates sulphur dioxide ($SO_2$) by reacting with water (Eq. 2) [54]. Since PDMS is gas permeable, $SO_2$ could cross PDMS membrane and influence the significance of generation of hypoxia on the microchip system.

$$2Na_2SO_3 + O_2 \longrightarrow 2Na_2SO_4 \tag{1}$$

$$Na_2SO_3 + H_2O \longrightarrow SO_2 + 2NaOH \tag{2}$$

Although we were unable to measure the exact level of hypoxia on the microchips along with RNA analyses, our previous studies support low oxygen levels ($O_2 \leq 5\%$) produced by the microchip [22,23].

It also remains possible that Myogel prevented or modulated the expected effects of the oxygen scavenger. Remarkably, uterine myomas might be hypoxic as such [55], and this could further interfere with the
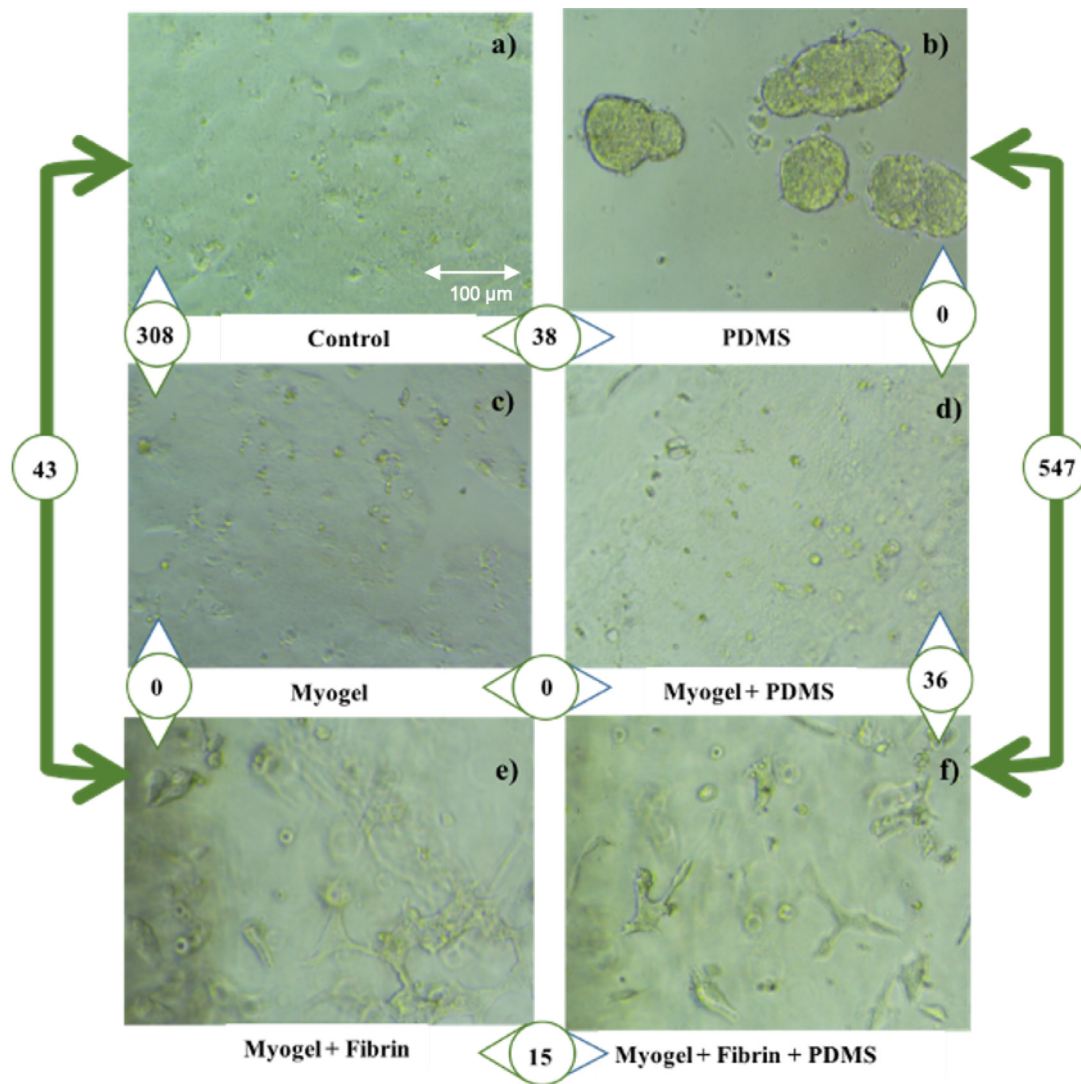
**Fig. 3.** Morphology and the number of significantly differentially expressed genes in JEG-3 cells in the cultures a) Control (only medium),308 significant gene expressed in Myogel over control, 38 genes expressed in PDMS over control, 43 genes expressed in Myogel + Fibrin over control. b) PDMS,not significant genes expressed between PDMS and Myogel + PDMS, 547 genes expressed in Myogel + Fibrin + PDMS over PDMS. c) Myogel,not significant genes expressed in Myogel + Fibrin over Myogel and Myogel + PDMS over Myogel. d) Myogel + PDMS,36 genes expressed in Myogel + Fibrin + PDMS over Myogel + PDMS. e) Myogel + fibrin,15 genes expressed in Myogel + Fibrin + PDMS over Myogel + Fibrin. f) Myogel + fibrin + PDMS. Three replicates from each condition (n=3).

**Table 2**

14 genes that were differentially expressed both in our microchip experiment and in the dataset of Zhu et al. Log2 fold changes and adjusted P-values are compared, and known pathways involved are shown.

| DE genes in both sets | Our study | | Zhu et al. | | MSigDB pathways involved (Enrichr) | | | | | | | |
|---|---|---|---|---|---|---|---|---|---|---|---|---|
| | log2 FC | p(adj) | log2 FC | p(adj) | Hypoxia | mTORC1 Signaling | Myc Targets V1 | p53 Pathway | Apoptosis | Glycolysis | E2F Targets | G2-M Checkpoint |
| RPS27 | 1.24 | 5.15E-08 | 1.01 | 3.33E-02 | | | | | | | | |
| FTH1 | 1.10 | 6.86E-05 | 1.43 | 2.85E-04 | | | | | | | | |
| RPS24 | 0.93 | 2.65E-04 | 1.03 | 2.54E-02 | | | | | | | | |
| CANX | 1.00 | 4.43E-04 | 1.56 | 1.07E-02 | | x | x | | | | | |
| RPS27A | 0.76 | 2.04E-03 | 1.33 | 1.70E-02 | | | | | | | | |
| GAPDH | 0.84 | 2.22E-03 | 1.85 | 7.22E-07 | x | x | | | | | x | |
| HMGB2 | 0.76 | 5.35E-03 | 3.63 | 3.82E-04 | | | | | x | | x | |
| JUND | 0.71 | 1.14E-02 | 1.82 | 1.89E-03 | | | | | | | | |
| SFPQ | 0.65 | 1.22E-02 | 2.32 | 2.26E-03 | | | | | | | | x |
| CCSAP | 0.63 | 1.87E-02 | 1.90 | 1.46E-02 | | | | | | | | |
| GM2A | 0.56 | 2.88E-02 | 1.52 | 2.07E-03 | | | | x | | | | |
| ENO1 | 0.52 | 3.06E-02 | 4.22 | 3.98E-14 | x | x | | | | x | | |
| RACK1 | 0.59 | 3.85E-02 | 1.01 | 3.66E-02 | | | x | | | | | |
| TPI1 | 0.57 | 4.59E-02 | 1.29 | 6.59E-03 | x | x | | | | x | | |

effects of the hypoxia on Myogel coated microchips in comparison with the previous studies.

## 5. Conclusion

This study shows that JEG-3 cells cultured on the Myogel matrix associate with strong stimulation of ribosomal pathways, energy metabolism, and ATP production. Myogel matrix provides better JEG-3 cell adherence on PDMS and shows significant effects on cell morphology and RNA expression. Although our results did not show significant upregulation of the hypoxia pathway genes using the oxygen scavenger and the microchip setup, significant upregulation of several individual hypoxia-related genes and the oxidative phosphorylation pathway arose. These results provide important insights into the possibility to modulate cellular processes and gene expression by different coating. Moreover, our results support the utility of cellular microenvironments in JEG-3 studies. Further studies are needed to assess the effects of temporary and chronic hypoxia in the cell morphology, invasive capacity, and gene expression.

### Declaration of Competing Interest

The authors declare the following financial interests/personal relationships which may be considered as potential competing interests:

Sameeineh Barmaki reports financial support was provided by University of Helsinki. Sameeineh Barmaki reports a relationship with University of Helsinki that includes: employment and funding grants.

### Supplementary material

Supplementary material associated with this article can be found, in the online version, at doi:10.1016/j.bbiosy.2022.100056.

## References

[1] Soares MJ, Varberg KM, Iqbal K. Hemochorial placentation: development, function, and adaptations. Biol Reprod 2018;99(1):196–211. doi:10.1093/biolre/ioy049.

[2] Semenza GL. Oxygen homeostasis. WIREs Syst Biol Med 2010;2(3):336–61. doi:10.1002/wsbm.69.

[3] Hu X-Q, Zhang L. Hypoxia and mitochondrial dysfunction in pregnancy complications. Antioxidants 2021;10(3). doi:10.3390/antiox10030405.

[4] Burton GJ. Oxygen, the janus gas; its effects on human placental development and function. J Anat 2009;215(1):27–35.

[5] Tal R, Shaish A, Barshack I, Polak-Charcon S, Afek A, Volkov A, Feldman B, Avivi C, Harats D. Effects of hypoxia-inducible factor-1alpha overexpression in pregnant mice: possible implications for preeclampsia and intrauterine growth restriction. Am J Pathol 2010;177(6):2950–62.

[6] Soares MJ, Iqbal K, Kozai K. Hypoxia and placental development. Birth Defects Research 2017;109:1309–29. doi:10.1002/bdr2.1135.

[7] Soleymanlou N, Jurisica I, Nevo O, Ietta F, Zhang X, Zamudio S, Post M, Caniggia I. Molecular evidence of placental hypoxia in preeclampsia. J Clin Endocrinol Metab 2005;90(7):4299–308.

[8] Fisher SJ. Why is placentation abnormal in preeclampsia? Am J Obstet Gynecol 2015;213(4 Suppl):S115–22.

[9] Garziera M, Scarabel L, Toffoli G. Hypoxic modulation of HLA-G expression through the metabolic sensor HIF-1 in human cancer cells. J Immunol Res 2017;2017:4587520.

[10] Lee CQ, Gardner L, Turco M, Zhao N, Murray MJ, Coleman N, et al. What is trophoblast? A combination of criteria define human first-trimester trophoblast. Stem Cell Rep 2016;6(2):257–72.

[11] Byrne M, Leslie M, Gaskins R, Kenis P. Methods to study the tumor microenvironment under controlled oxygen conditions. Trends Biotechnol 2014;32. doi:10.1016/j.tibtech.2014.09.006.

[12] Bilban M, Tauber S, Haslinger P, Pollheimer J, Saleh L, Pehamberger H, Wagner O, Knöfler M. Trophoblast invasion: assessment of cellular models using gene expression signatures. Placenta 2010;31(11):989–96.

[13] Qian Zhang, Zhenzhen Wang XCHW. Lncrna dancr promotes the migration an invasion and of trophoblast cells through microrna-214-5p in preeclampsia. Bioengineered 2021;12:9424–34. doi:10.1080/21655979.2021.1988373.

[14] Mikhailova V, Khokhlova E, Grebenkina P, Salloum Z, Nikolaenkov I, Markova K, Davidova A, Selkov S, Sokolov D. Nk-92 cells change their phenotype and function when cocultured with il-15, il-18 and trophoblast cells. Immunobiology 2021;226:152125. doi:10.1016/j.imbio.2021.152125.

[15] Murrieta-Coxca JM, Gutiérrez-Samudio RN, El-Shorafa HM, Groten T, Rodríguez-Martínez S, Cancino-Diaz ME, et al. Role of il-36 cytokines in the regulation of angiogenesis potential of trophoblast cells. Int J Mol Sci 2020;22:285. doi:10.3390/ijms22010285.

[16] Patel J, Landers K, Mortimer RH, Richard K. Regulation of hypoxia inducible factors (HIF) in hypoxia and normoxia during placental development. Placenta 2010;31(11):951–7.

[17] Strohmer H, Kiss H, Mösl B, Egarter C, Husslein P, Knöfler M. Hypoxia downregulates continuous and interleukin-1-induced expression of human chorionic gonadotropin in choriocarcinoma cells. Placenta 1997;18(7):597–604.

[18] Taylor CM, Stevens H, Anthony FW, Wheeler T. Influence of hypoxia on vascular endothelial growth factor and chorionic gonadotrophin production in the trophoblast-derived cell lines: jeg, jar and bewo. Placenta 1997;18(5–6).

[19] Shin BS, Kim HG, Choi OH. Mitochondrial channel opener diazoxide attenuates hypoxia-induced sFlt-1 release in human choriocarcinoma cells. J Menopausal Med 2014;20(1):21–31.

[20] Qu HM, Qu LP, Li XY, Pan XZ. Overexpressed HO-1 is associated with reduced STAT3 activation in preeclampsia placenta and inhibits STAT3 phosphorylation in placental jeg-3 cells under hypoxia. Arch Med Sci 2018;14(3):597–607.

[21] Zhao J, Chow RP, McLeese RH, Hookham MB, Lyons TJ, Yu JY. Modelling preeclampsia: a comparative analysis of the common human trophoblast cell lines. FASEB Bioadv 2021;3(1):23–35.

[22] Barmaki S, Jokinen V, Obermaier D, Blokhina D, Korhonen M, Ras RHA, Vuola J, Franssila S, Kankuri E. A microfluidic oxygen sink to create a targeted cellular hypoxic microenvironment under ambient atmospheric conditions. Acta Biomater 2018;73:167–79.

[23] Barmaki S, Obermaier D, Kankuri E, Vuola J, Franssila S, Jokinen V. A microfluidic chip architecture enabling a hypoxic microenvironment and nitric oxide delivery in cell culture. Micromachines (Basel) 2020;11(11). doi:10.3390/mi1110979.

[24] Salo T, Sutinen M, Hoque Apu E, Sundquist E, Cervigne NK, de Oliveira CE, Akram SU, Ohlmeier S, Suomi F, Eklund L, Juusela P, Åström P, Bitu CC, Santala M, Savolainen K, Korvala J, Paes Leme AF, Coletta RD. A novel human leiomyoma tissue derived matrix for cell culture studies. BMC Cancer 2015;15:981.

[25] Salo T, Dourado MR, Sundquist E, Apu EH, Alahuhta I, Tuomainen K, Vasara J, Al-Samadi A. Organotypic three-dimensional assays based on human leiomyoma-derived matrices. Philos Trans R Soc Lond B Biol Sci 2018;373(1737).

[26] Nishi H, Nakada T, Hokamura M, Osakabe Y, Itokazu O, Huang LE, Isaka K. Hypoxia-inducible factor-1 transactivates transforming growth factor-beta3 in trophoblast. Endocrinology 2004:4113–18.

[27] Sun H, Zhao A, Li M, Dong H, Sun Y, Zhang X, Zhu Q, Bukhari AA, Cao C, Su D, Liu Y, Liang X. Interaction of calcium binding protein S100A16 with myosin-9 promotes cytoskeleton reorganization in renal tubulointerstitial fibrosis. Cell Death Dis 2020;11(2):146.

[28] Hatchell EC, Colley SM, Beveridge DJ, Epis MR, Stuart LM, Giles KM, et al. Slirp, a small sra binding protein, is a nuclear receptor corepressor. Mol Cell 2006;22(5):657–68.

[29] Love MI, Huber W, Anders S. Moderated estimation of fold change and dispersion for RNA-seq data with DESeq2. Genome Biol 2014;15(12):550.

[30] Sasagawa T, Nagamatsu T, Morita K, Mimura N, Iriyama T, Fujii T, Shibuya M. HIF-2$\alpha$, but not HIF-1$\alpha$, mediates hypoxia-induced up-regulation of Flt-1 gene expression in placental trophoblasts. Sci Rep 2018;8(1):17375.

[31] Kim JS, Choi YS, Park JH, Yun J, Kim S, Lee JH, et al. Role of B-cell translocation gene 1 in the pathogenesis of endometriosis. Int J Mol Sci 2019;20(13).

[32] Robinson MD, McCarthy DJ, Smyth GK. Edger:a bioconductor package for differential expression analysis of digital gene expression data. Bioinformatics 2010;26:139–40. doi:10.1093/bioinformatics/btp616.

[33] Kallio MA, Tuimala JT, Hupponen T, Klemelä P, Gentile M, Scheinin I, Koski M, Käki J, Korpelainen EI. Chipster: user-friendly analysis software for microarray and other high-throughput data. BMC Genomics 2011;12:507.

[34] Babicki S, Arndt D, Marcu A, Liang Y, Grant JR, Maciejewski A, Wishart DS. Heatmapper: web-enabled heat mapping for all. Nucleic Acids Res 2016. doi:10.1093/nar/gkw419.

[35] Chen EY, Tan CM, Kou Y, Duan Q, Wang Z, Meirelles GV, Clark NR, Ma'ayan A. Enrichr: interactive and collaborative HTML5 gene list enrichment analysis tool. BMC Bioinformatics 2013;14:128.

[36] Wahbi W, Naakka E, Tuomainen K, Suleymanova I, Arpalahti A, Miinalainen I, et al. The critical effects of matrices on cultured carcinoma cells: human tumor-derived matrix promotes cell invasive properties. Exp Cell Res 2020;389(1):111885.

[37] Kuleshov MV, Jones MR, Rouillard AD, Fernandez NF, Duan Q, Wang Z, Koplev S, Jenkins SL, Jagodnik KM, Lachmann A, McDermott MG, Monteiro CD, Gundersen GW, Ma'ayan A. Enrichr: a comprehensive gene set enrichment analysis web server 2016 update. Nucleic Acids Res 2016;44(W1):W90–7.

[38] Cui Y, Li L, Li Z, Yin J, Lane J, Ji J, Jiang WG. Dual effects of targeting S100A11 on suppressing cellular metastatic properties and sensitizing drug response in gastric cancer. Cancer Cell Int 2021;21(1):243.

[39] Berg J, Tymoczko J, Stryer L. Biochemistry, fifth edition. WH Freeman; 2002. ISBN 9780716730514. https://books.google.se/books?id=uDFqAAAAMAAJ

[40] Blagosklonny M. Hypoxia, mtor and autophagy. Autophagy 2012;9. doi:10.4161/auto.22783.

[41] Duronio RJ, Xiong Y. Signaling pathways that control cell proliferation. Cold Spring Harb Perspect Biol 2013;5 3:a008904.

[42] Ding W, Fan XL, Xu X, Huang JZ, Xu SH, Geng Q, et al. Epigenetic silencing of ITGA2 by MiR-373 promotes cell migration in breast cancer. PLoS ONE 2015;10(8):e0135128.

[43] Bassler J, Hurt E. Eukaryotic ribosome assembly. Annu Rev Biochem 2019;88. doi:10.1146/annurev-biochem-013118-110817.

[44] Papandreou I, Cairns RA, Fontana L, Lim AL, Denko NC. HIF-1 mediates adaptation to hypoxia by actively downregulating mitochondrial oxygen consumption. Cell Metab 2006;3(3):187–97.

[45] Kim JW, Gao P, Liu YC, Semenza GL, Dang CV. Hypoxia-inducible factor 1 and dysregulated c-Myc cooperatively induce vascular endothelial growth factor and metabolic switches hexokinase 2 and pyruvate dehydrogenase kinase 1. Mol Cell Biol 2007;27(21):7381–93.

[46] Sun HX, Xu Y, Yang XR, Wang WM, Bai H, Shi RY, Nayar SK, Devbhandari RP, He YZ, Zhu QF, Sun YF, Hu B, Khan M, Anders RA, Fan J. Hypoxia inducible factor 2 alpha inhibits hepatocellular carcinoma growth through the transcription factor dimerization partner 3/ E2F transcription factor 1-dependent apoptotic pathway. Hepatology 2013;57(3):1088–97.

[47] Hubbi M, Semenza G. Regulation of cell proliferation by hypoxia-inducible factors. Am J Physiol Cell Physiol 2015;309. doi:10.1152/ajpcell.00279.2015.

[48] Godet I, Shin YJ, Ju JA, Ye IC, Wang G, Gilkes DM. Fate-mapping post-hypoxic tumor cells reveals a ROS-resistant phenotype that promotes metastasis. Nat Commun 2019;10(1):4862.

[49] Baluapuri A, Wolf E, Eilers M. Target gene-independent functions of MYC oncoproteins. Nat Rev Mol Cell Biol 2020;21(5):255–67.

[50] Hu XQ, Zhang L. Hypoxia and mitochondrial dysfunction in pregnancy complications. Antioxidants (Basel) 2021;10(3).

[51] Holland O, Dekker Nitert M, Gallo LA, Vejzovic M, Fisher JJ, Perkins AV. Review: placental mitochondrial function and structure in gestational disorders. Placenta 2017;54:2–9.

[52] Zhu L; Lv R.. Effect of hypoxia in severe preeclampsia through epigenetic regulation. https://www.ncbi.nlm.nih.gov/geo/query/acc.cgi?acc=GSE72437; 2017.

[53] Marino K, Silva E, Windelborn J. A comparison between chemical and gas hypoxia as models of global ischemia in zebrafish (danio rerio). Anim Model Exper Med 2020;3. doi:10.1002/ame2.12132.

[54] Bin J, Ren C, Li Y, Lu Y, Li W, Wu Y, et al. Sodium sulfite is a potential hypoxia inducer that mimics hypoxic stress in caenorhabditis elegans. J Biol Inorg Chem 2010;16:267–74. doi:10.1007/s00775-010-0723-1.

[55] Teppo S, Sundquist E, Vered M, Holappa H, Parkkisenniemi J, Rinaldi TA, et al. The hypoxic tumor microenvironment regulates invasion of aggressive oral carcinoma cells. Exp Cell Res 2013;319 4:376–89.